Chapter 3

CIRCULARLY POLARIZED ANTENNAS

In this chapter, three types of rectangular-cavity-backed slot antennas are proposed to radiate circularly polarized waves. Characteristics such as input impedance, VSWR, axial ratio and radiation pattern are investigated. The effect of the structural dimensions on the antenna characteristics is discussed.

For simplicity, the square cavities, i.e. Xc=Yc, are chosen in all calculations, although the formulation as stated in Chapter 2 is not limited to the square cavity. In the Galerkin's procedure, the slot is divided into small segments around $\lambda_0/20$ (λ_0 is the wavelength at a center frequency f_0), and f_0 is selected at which the axial ratio becomes minimum. The magnitude of the magnetic current given in this chapter is normalized by the magnetic current at the feed point.

The calculations in this chapter are based on the formulation derived in Chapter 2. The calculations of magnetic currents and input impedance are according to Eqs. (2.18) and (2.30) of Chapter 2. The calculation of axial ratio (AR) is according to Eq. (A.21) of Appendix.

To ensure the validity of the numerical results, the calculated input impedance, axial ratio and radiation pattern are compared with the experimental results.

3.1 Rectangular-Cavity-Backed Single Square Loop Slot Antenna

3.1.1 Antenna Structure

As an entry to the analysis, we consider the simplest rectangularly bent loop slot antenna which is the rectangular-cavity-backed single square loop slot antenna. We denote the two side lengths of the square loop slot as Xs and Ys, respectively. In this section, the single square loop slot, i.e. Xs=Ys, is only considered, and is placed at the center of the cavity on the ground plane as shown in Fig. 3.1.

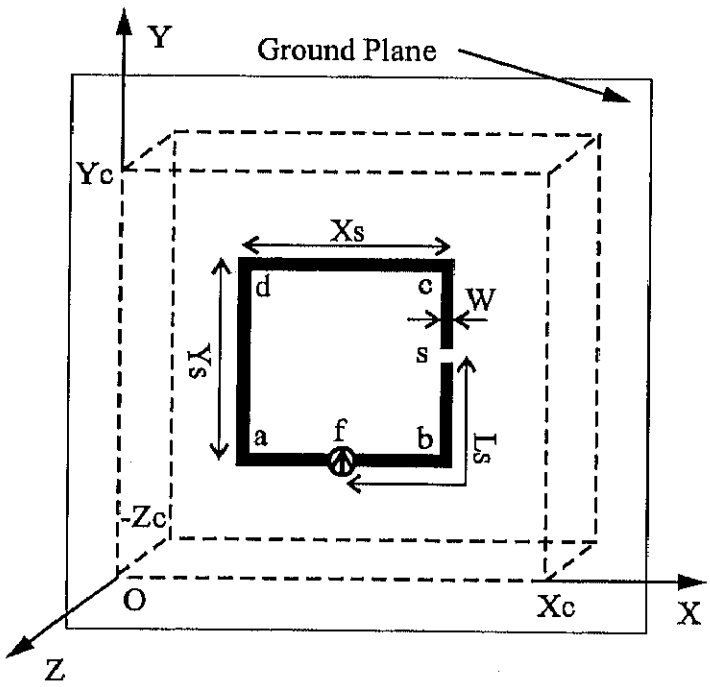

Fig. 3.1: Rectangular-cavity-backed single square loop slot antenna.

A constant current i_0 is fed across the slot at one center of the slot side, i.e. the point (Xc/2, (Yc-Ys)/2, 0). A short-circuiting point where $\vec{M} = 0$ is set at the slot, and the distance from the feed point to the short-circuiting point along the slot is denoted as Ls. By adjusting the position of the short-circuiting

point, circularly polarized waves are expected to radiate.

3.1.2 Conditions for Circular Polarization

To radiate circularly polarized waves, a loop slot antenna needs to have a traveling wave magnetic current distribution, which has constant amplitude and linearly changing phase. In the reference [20], the circular loop slot antenna with over one wavelength perimeter can radiate circularly polarized waves by means of short-circuiting the slot. To have a short-circuiting point is a very simple method and it is clarified that suitable parameters for the perimeter of the loop and the short-circuiting position exist to radiate a circularly polarized wave. To have a short-circuiting point across the slot is equivalent to load an infinitely large reactance. The short-circuiting point interrupts magnetic current distribution along the slot and at some specific short-circuiting position the circular polarization is expected to exist.

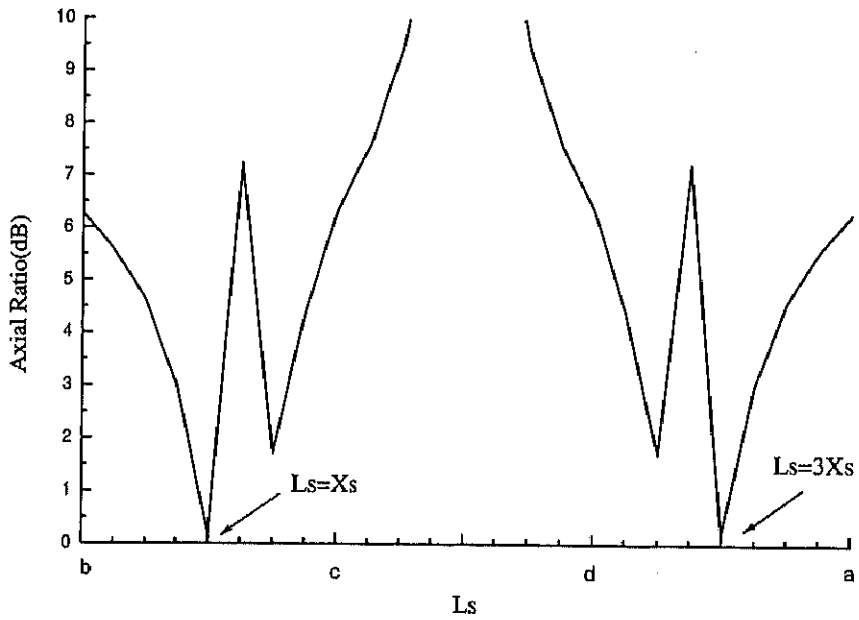

Fig. 3.2: Axial ratio in the Z direction against a short-circuiting position, where Xc=Yc=145mm, Zc=13mm, Xs=Ys=81mm, W=3mm, f_0=1.56GHz.

Fig. 3.2 shows the axial ratio in the Z direction against a short-circuiting position Ls at f_0=1.56GHz. From this figure, we can see that the AR varies greatly with the short-circuiting position. This implies that the magnetic current distribution is strongly affected by the short-circuiting point. When the short-circuiting point is set at Ls=Xs (=81mm) or 3Xs, the AR reaches to its lowest value of 0.18dB. Note that the two short-circuiting points are always symmetrical to the feed point and the senses of the polarization for the two short-circuiting points are opposite.

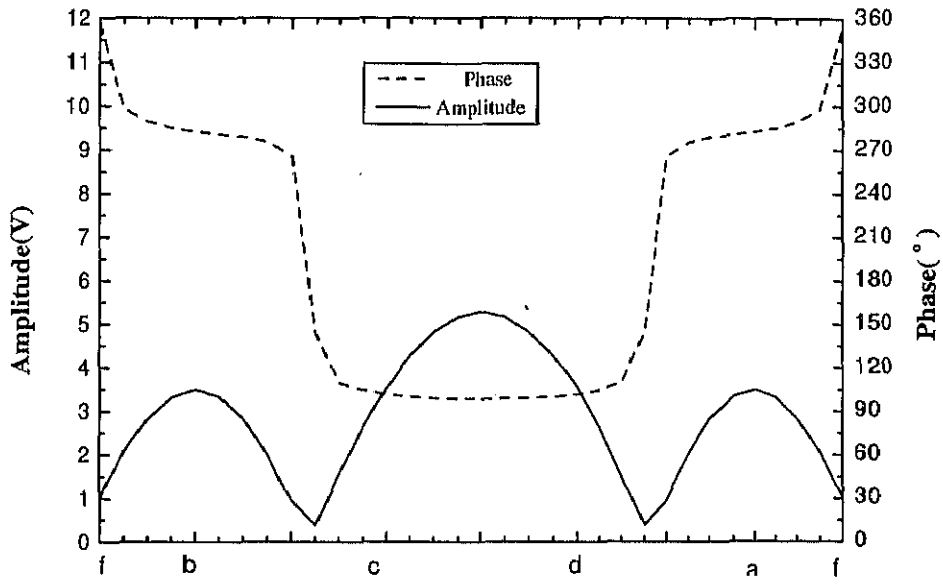

Fig. 3.3: Magnetic current distribution along the slot without a short-circuiting point, where Xc=Yc=145mm, Zc=13mm, Xs=Ys=81mm, W=3mm, f_0=1.56GHz.

The calculated magnetic current amplitude and phase for the case without the short-circuiting point are shown in Fig. 3.3. In the calculation, the electric current source of 1 A is assumed and the amplitude of the magnetic current is normalized to the amplitude of the magnetic current at the feed point. It is seen that a typical standing wave magnetic current is excited on the slot.

The introduction of a short-circuiting point to the slot will interrupt magnetic current distribution along the slot. The influence of the short-circuiting

on the polarization characteristics can be investigated through this magnetic current distribution.

The square loop slot with a short-circuiting point (point "s"), as shown in Fig. 3.1, can be treated as two slot elements, i.e. a long slot element "s-c-d-a-f" and a short slot element "f-b-s". Its calculated magnetic current distribution and the contributions of the magnetic currents to the far field are shown in Figs. 3.4 and 3.5, respectively. Along the long slot element "s-c-d-a-f", a traveling wave magnetic current distribution (linearly changing phase) is dominant (see Fig. 3.4), and its contribution to the far field is an elliptically polarized wave E_{tw}. While along the short slot element "f-b-s", a standing wave magnetic current distribution (constant phase) is dominant, and its contribution to the far field is a linearly polarized wave E_{sw}. The total far field E_{total} (the composition of elliptically polarized and linearly polarized waves) is elliptically polarized. Thus, by adjusting the short-circuiting position (i.e. adjusting the standing wave component due to the short slot and the traveling wave component due to the long slot), circular polarization can be obtained (see Figs. 3.2, 3.4 and 3.5).

For the rectangular-cavity-backed single square loop slot antenna, the optimized antenna dimensions for the circular polarization at $f_0 = 1.56$GHz (λ_0 = 192.3mm) are summarized in Table 3.1. From this table we can see that circular polarization occurs when the short-circuiting point is set $0.421\lambda_0$ from the feed point. The dimensions of the cavity also contribute to the occurrence of the circular polarization as can be seen in the next subsection.

Xc	Zc	4Xs	Ls
$0.754\lambda_0$	$0.0676\lambda_0$	$1.69\lambda_0$	$0.421\lambda_0$

Table 3.1: Optimized antenna dimensions for circular polarization.

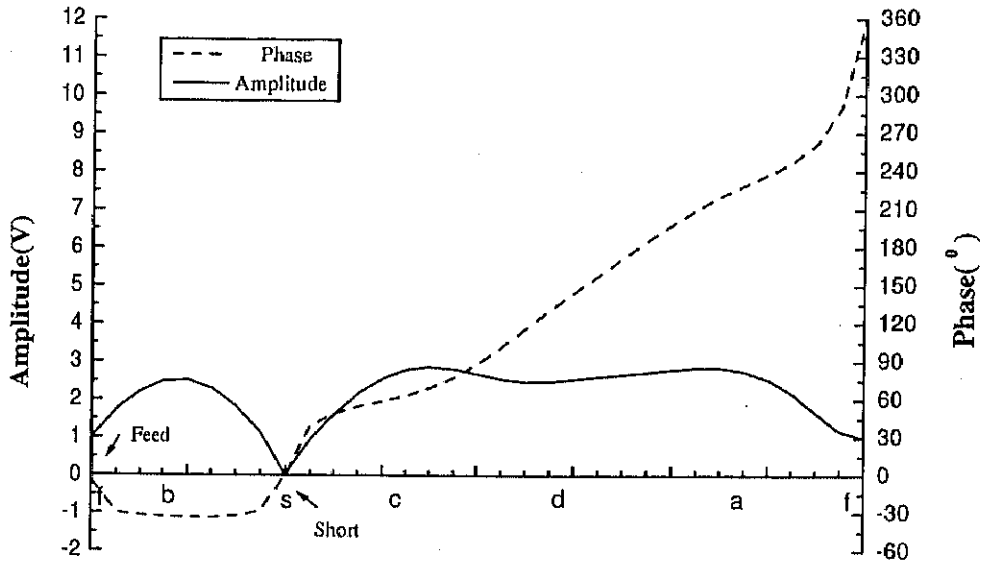

Fig. 3.4: Magnetic current distribution along the slot with a short-circuiting point, where Xc=Yc=145mm, Zc=13mm, Xs=Ys=81mm, W=3mm, Ls=81mm, f_0=1.56GHz.

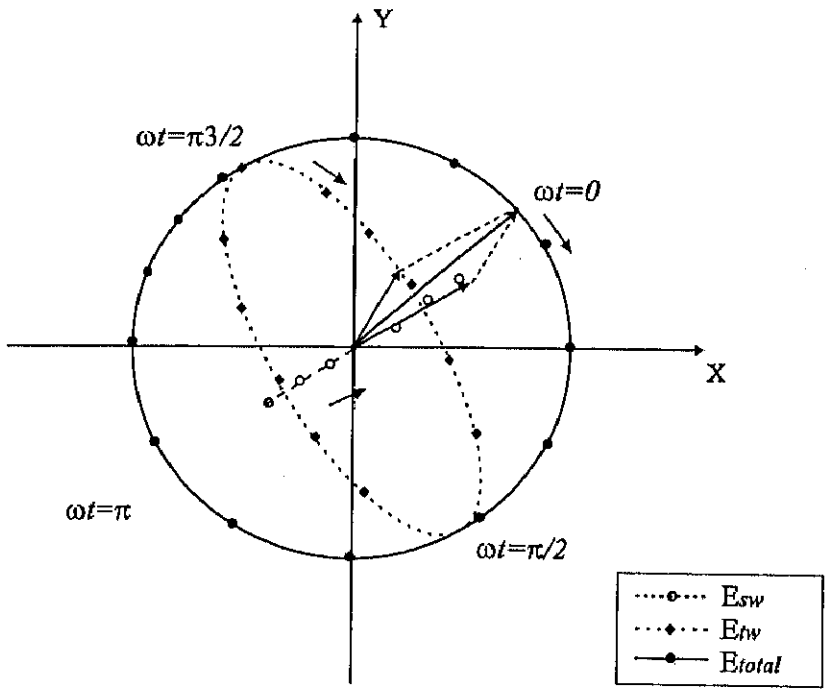

Fig. 3.5: Trace of the far zone electric field vector.

3.1.3 Antenna Characteristics

In this subsection, the characteristics of the rectangular-cavity-backed single square loop slot antenna will be discussed. The frequency band is selected around the center frequency f_0=1.56GHz.

A slot antenna without a cavity can radiate into two directions. When the slot is backed by a cavity, it can radiate only in one direction and the input impedance characteristics will also be affected. This variation can be seen in Fig. 3.6. From this figure we can see that when the slot is backed by a cavity, both of the absolute value of input resistance and inductance decrease in the frequency region around the center frequency f_0=1.56GHz. If the cavity dimensions and the slot are properly adjusted, the input capacitance of the slot can cancel the input inductance of the cavity, so that the input impedance becomes purely resistive.

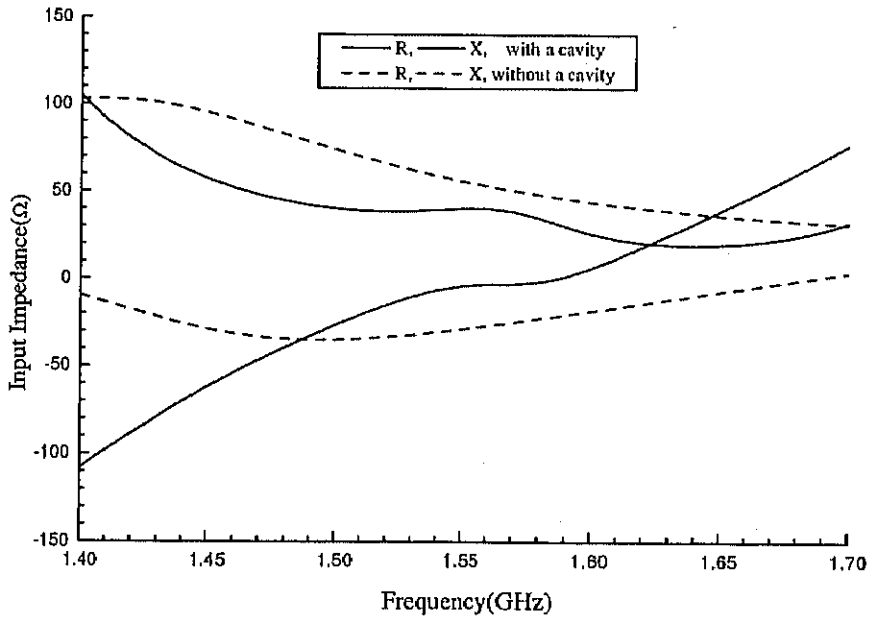

Fig. 3.6: Input impedance against frequency with a short-circuiting point, where Xc=Yc=145mm, Zc=13mm, Xs=Ys=81mm, W=3mm, Ls=81mm.

For the case with a short-circuiting point, the input impedance against

frequency is given in Figs. 3.7 and 3.8. In Fig. 3.7, the different cavity depth Zc's 9mm, 13mm, and 17mm are chosen, respectively. In Fig. 3.8, the cavity width Xc's are 140mm, 145mm, and 150mm, respectively. It is obvious that the effect of the cavity depth Zc on the input impedance is more significant than that of the cavity width Xc.

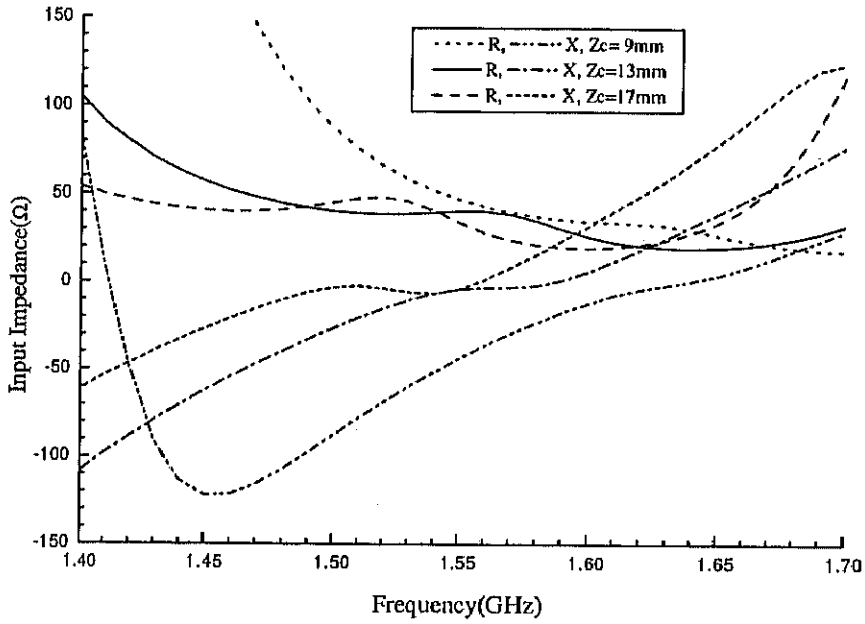

Fig. 3.7: Input impedance against frequency with a short-circuiting point, where Xc=Yc=145mm, Xs=Ys=81mm, W=3mm, Ls=81mm.

For the circularly polarized antennas, the axial ratio is very important. Figs. 3.9 and 3.10 show the axial ratio in the Z direction against frequency. For comparison, the axial ratio for the antenna with and without a cavity are plotted in Fig. 3.9. It is observed that the larger the cavity depth, the lower the center frequency. The antenna without the cavity is the special case that the cavity depth tends to be infinitely large. When $Xc=0.756\lambda_0$, $Zc=0.0676\lambda_0$ and the total length of the slot is $1.685\lambda_0$ (f_0=1.56GHz), the minimum axial ratio of 0.18 dB is obtained. The axial ratio bandwidth ($\leq$ 3dB) of the rectangular-cavity-backed antenna decreases to about 2% from 5% of that without the cavity. In Fig. 3.10, the calculated axial ratios for the different cavity widths

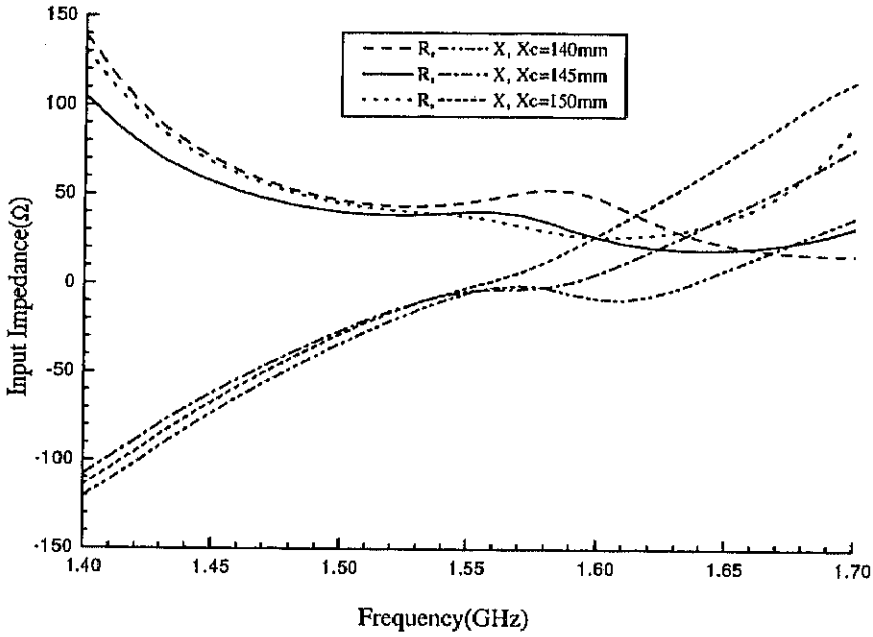

Fig. 3.8: Input impedance against frequency with a short-circuiting point, where Zc=13mm, Xs=Ys=81mm, W=3mm, Ls=81mm.

Xc's are shown. It is found that the axial ratio is very sensitive to the cavity width.

Figs. 3.11 and 3.12 show the computed radiation patterns and the axial ratios with respect to θ in the $\phi = 0°$, 45°, 90° and 135° planes, respectively. The operating frequency is chosen as 1.56GHz. Because of the unsymmetrical structure of the slot, the radiation patterns are unsymmetrical. It should be noted that the E_θ maximum in the $\phi = 90°$ plane and the E_ϕ maximum in the $\phi = 45°$ plane have a shift of 10 degrees from the zenith. The axial ratio is less than 3dB for $-30° \leq \theta \leq 30°$ in the $\phi = 0°$, 45° and 90° planes, while in the $\phi = 135°$ plane, the axial ratio is less than 3dB for $-70° \leq \theta \leq 70°$.

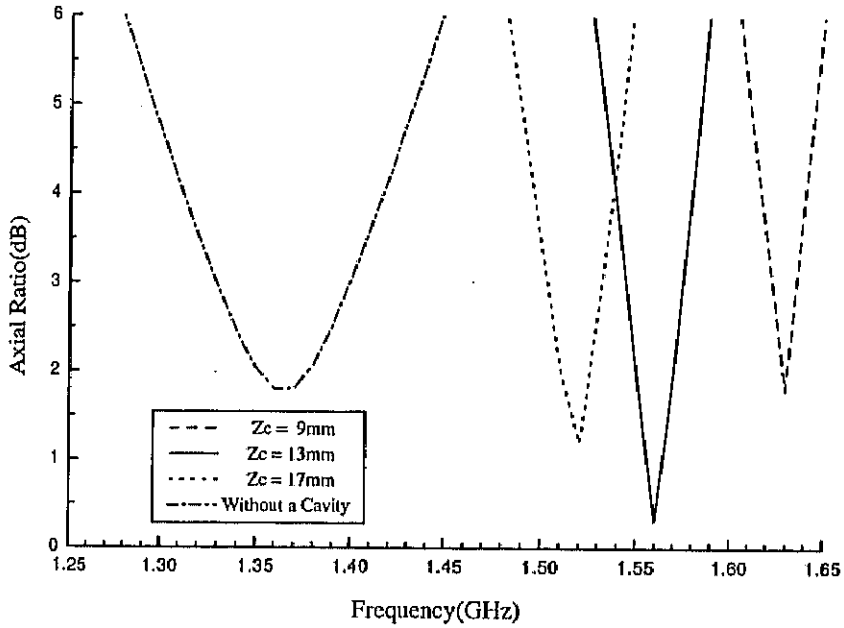

Fig. 3.9: Axial ratio for different Zc, where Xc=Yc=145mm, Xs=Ys=81mm, W=3mm, Ls=81mm.

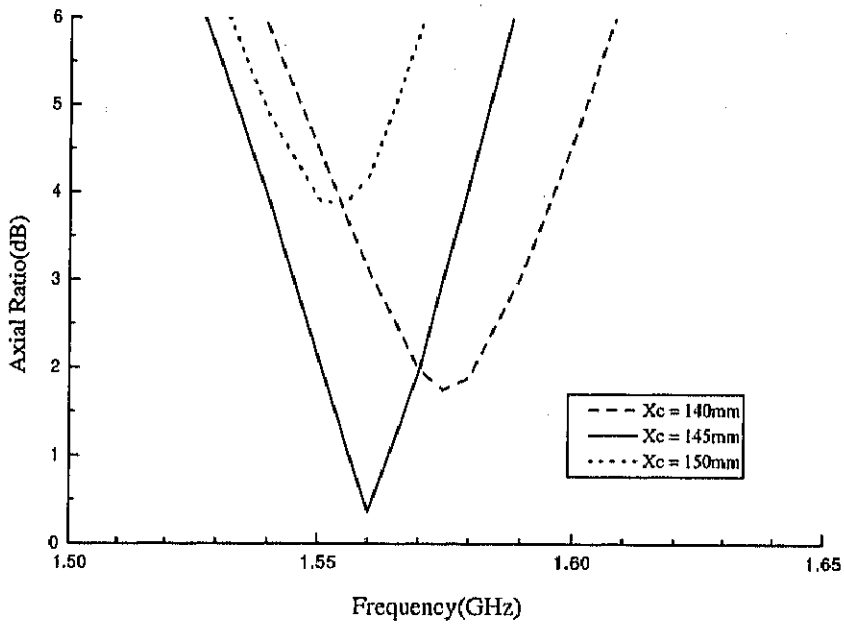

Fig. 3.10: Axial ratio for different Xc, where Zc=13mm, Xs=Ys=81mm, W=3mm, Ls=81mm.

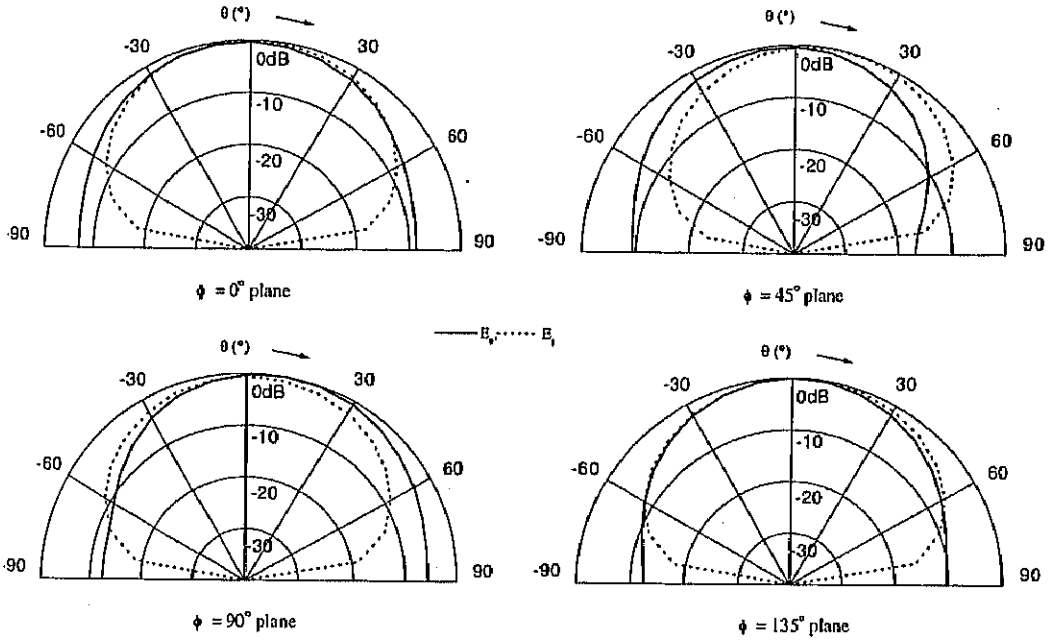

Fig. 3.11: Radiation patterns with a short-circuiting point, where Xc=Yc=145mm, Zc=13mm, Xs=Ys=81mm, W=3mm, Ls=81mm, f_0=1.56GHz.

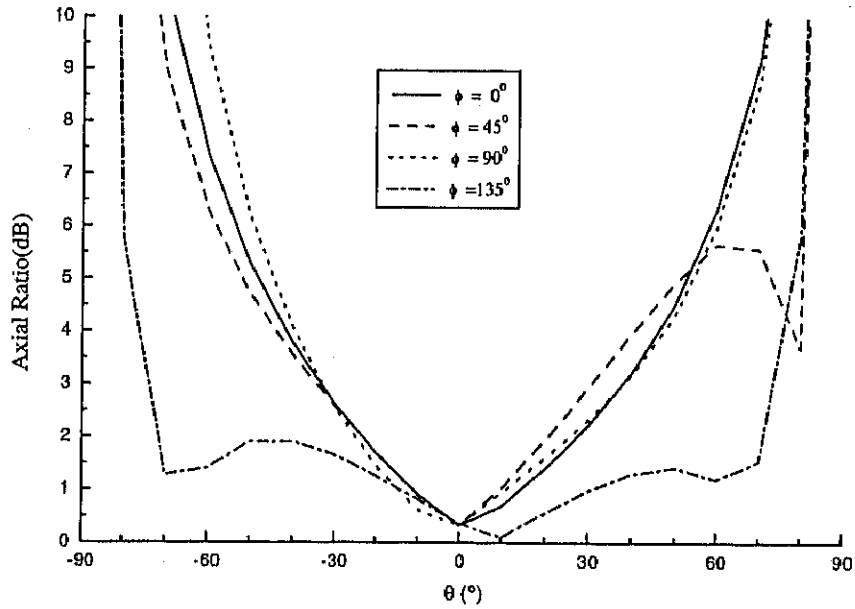

Fig. 3.12: Axial ratio with respect to θ in a constant φ plane, where Xc=Yc=145mm, Zc=13mm, Xs=Ys=81mm, W=3mm, Ls=81mm, f_0=1.56GHz.

3.1.4 Experimental Results

To verify the analysis, the experiment on characteristics of the input impedance, axial ratio and radiation pattern is performed. According to the discussion in the last subsection, the antenna dimensions are chosen as shown in Table 3.2. With these dimensions, the antenna is expected to radiate circularly polarized waves as calculated in the last subsection.

Xc	Yc	Zc	Xs	Ys	W	Ls
145mm	145mm	13mm	81mm	81mm	3mm	81mm

Table 3.2: Experimental dimensions of the rectangular-cavity-backed single square loop slot antenna.

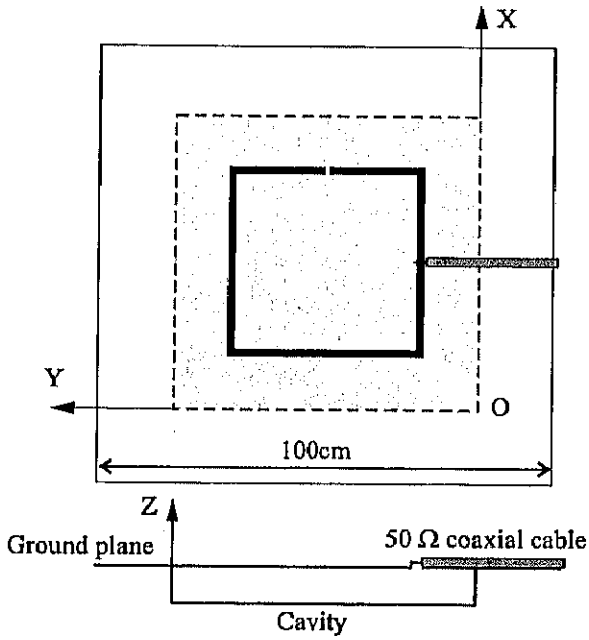

Fig. 3.13: Antenna structure in the experiment.

The antenna structure is shown in Fig. 3.13, where the antenna configuration and the way of feeding the slot by a 50 Ω semi-rigid coaxial cable are shown. In the experiment, a square copper plate with a side of 100cm and a thickness of 0.3mm is used as a ground plane. The square loop slot is formed

on the ground plane. The cavity is also made by the cooper plate of thickness 0.3mm. The slot is shorted with a cooper sheet of width 1mm. The slot is fed by a semi-rigid coaxial cable along the ground plane to minimize the effect of the feed line. The frequency used is the 1.56GHz band.

The measured and calculated input impedance and axial ratio are plotted in Figs. 3.14 and 3.15, respectively. From Figs. 3.14 and 3.15, we find that the measured and calculated input impedance and axial ratio are in good agreement.

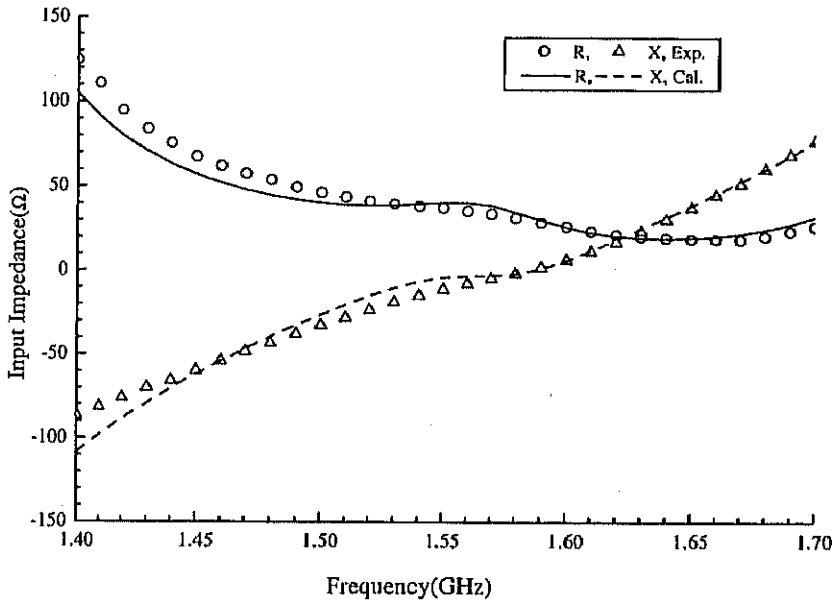

Fig. 3.14: The measured and calculated input impedance against frequency with a short-circuiting point, where Xc=Yc=145mm, Zc=13mm, Xs=Ys=81mm, W=3mm, Ls=81mm.

Fig. 3.16 shows the measured and calculated radiation patterns with respect to θ in the $\phi = 0°$ and 90° plane, respectively. The operating frequency is chosen as 1.56GHz. The calculated E_θ and E_ϕ in the $\phi = 0°$ and 90° plane are in good agreement with the measured results, except around $\theta = -90°$ and 90°. One of the reasons that the calculated results do not coincide with the measured ones around $\theta = -90°$ and 90° is the use of the finite-sized ground plane in the experiment.

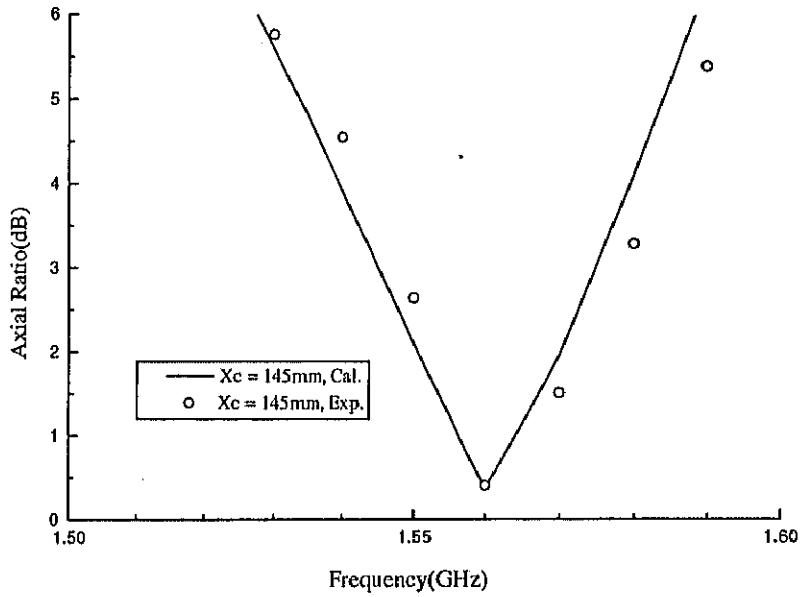

Fig. 3.15: The measured and calculated axial ratio against frequency with a short-circuiting point, where Xc=Yc=145mm, Zc=13mm, Xs=Ys=81mm, W=3mm, Ls=81.

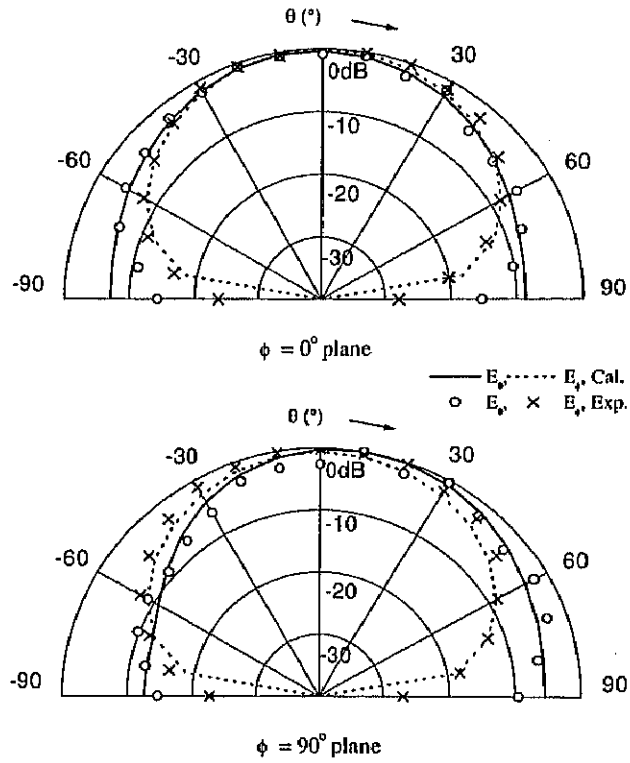

Fig. 3.16: The measured and calculated radiation patterns with a short-circuiting point, where Xc=Yc=145mm, Zc=13mm, Xs=Ys=81mm, W=3mm, Ls=81mm, f_0=1.56GHz.

3.2 Rectangular-Cavity-Backed Two-Element Square Loop Slot Antenna

Because of the unsymmetrical structure of the rectangular-cavity-backed single square loop slot antenna, the magnetic current distribution is unsymmetrical, and further, the radiation pattern has the shifted radiation pattern maximum of 5–10 degrees from the zenith (see Fig. 3.11). To overcome this asymmetry, a rectangular-cavity-backed two-element square loop slot antenna with the symmetry to its structure is proposed to radiate circularly polarized waves and in addition, to get the radiation pattern maximum in the zenith.

3.2.1 Antenna Structure

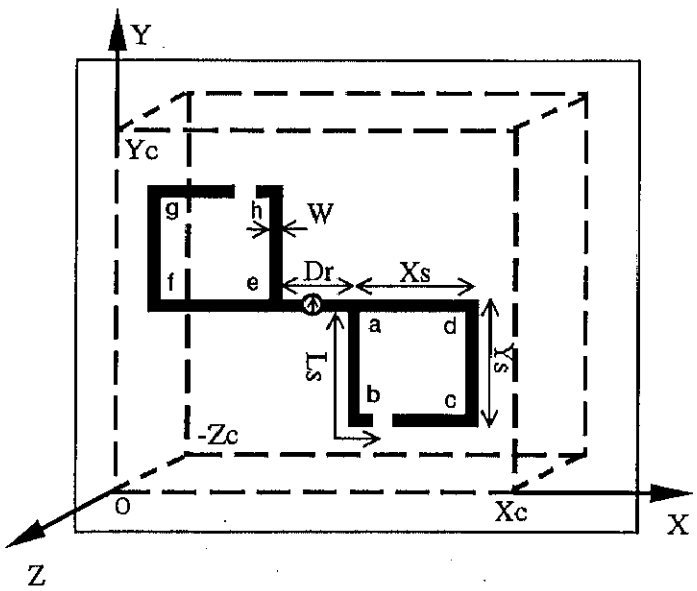

Fig. 3.17: A rectangular-cavity-backed two-element square loop slot antenna.

The rectangular-cavity-backed two-element square loop slot antenna is shown in Fig. 3.17, where Dr is the distance between the two rectangular loop slots. Xs and Ys are the length and the width of the rectangular loop slot,

respectively. The two-element rectangular loop slot is placed at the center of the cavity on the ground plane. The center frequency is chosen as f_0=1.6GHz. A constant current i_0 is fed across the center of the two-element rectangular loop slot at (Xc/2, Yc/2, 0). For simplicity, the square loop slot, i.e. Xs=Ys, is only considered. To obtain a symmetric traveling wave magnetic current distribution, two short-circuiting points where $\vec{M} = 0$ are set at the two positions (Ls) symmetric to the center of the slot (i.e. the feed point). By adjusting the short-circuiting positions, the circularly polarized waves will be produced by this traveling wave magnetic current.

3.2.2 Conditions for Circular Polarization

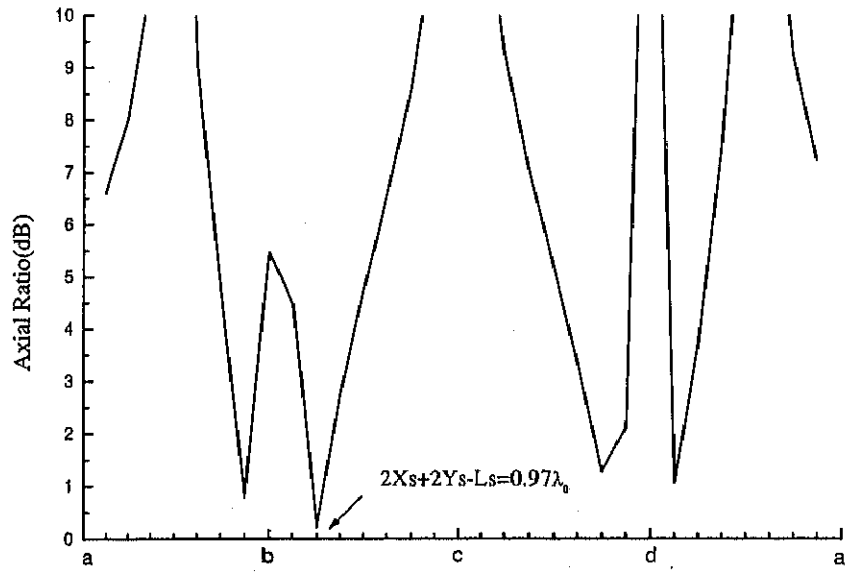

Fig. 3.18: Axial ratio in the Z direction against short-circuiting positions, where Xc=Yc=160mm, Zc=14mm, Xs=Ys=66mm, Dr=10mm, W=3mm, Ls=82mm, f_0=1.6GHz.

Just like the rectangular-cavity-backed single square loop slot antenna, the axial ratio is very sensitive to the short-circuiting position. The variation of the axial ratio in the Z direction against the short-circuiting position

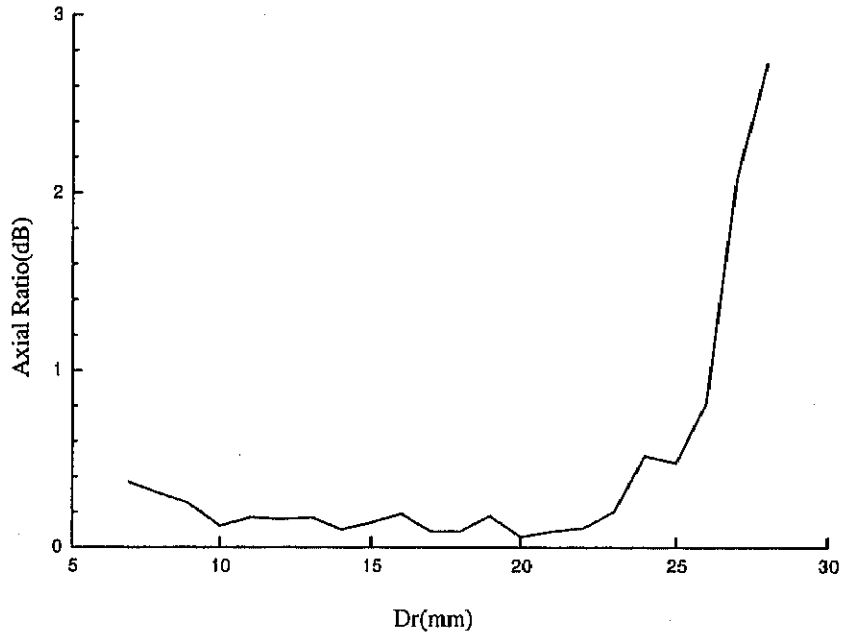

Fig. 3.19: Axial ratio in Z direction against Dr, where Xc=Yc=160mm, Zc=14mm, Xs=Ys=66mm, W=3mm, Ls=82mm, f_0=1.6GHz.

Ls is shown in Fig. 3.18. When the short-circuiting point is set at Ls=1.24Xs, i.e. 2Xs+2Ys-Ls=0.97λ_0, the axial ratio reaches its lowest value of 0.12dB. The axial ratio in the Z direction against Dr is shown in Fig. 3.19 where we can see that the axial ratio is not so sensitive to Dr, but it increases rapidly as the slot gets closer to the cavity wall. This means that the mutual coupling between the slot and the cavity wall becomes stronger when the slot gets closer to the cavity wall. The lowest axial ratio of 0.09dB is obtained at Dr=0.303Xs=20mm.

The calculated magnetic current amplitude and its phase are shown in Figs. 3.20 and 3.21. Fig. 3.20 is for the case without short-circuiting points. It is manifest that a typical standing wave magnetic current is excited on the slot. Due to the introduction of two short-circuiting points at points "Short1" and "Short2", traveling wave magnetic current distributions exist along the slot (points a $\rightarrow$ c $\rightarrow$ Short1 and points e $\rightarrow$ f $\rightarrow$ g $\rightarrow$ Short2) as shown in Fig. 3.21. The phase decreases linearly from the feed point to the two short-

circuiting points. It should be noted that the standing wave still exists along the slot (points Short1 → b → a → e → h → Short2). Because the slot structure is symmetric, the magnetic current amplitude and its phase for both Figs. 3.20 and 3.21 are symmetric with respect to the feed point. This kind of symmetric magnetic current distribution is expected to give better radiation pattern characteristics than that of the single rectangular loop slot structure.

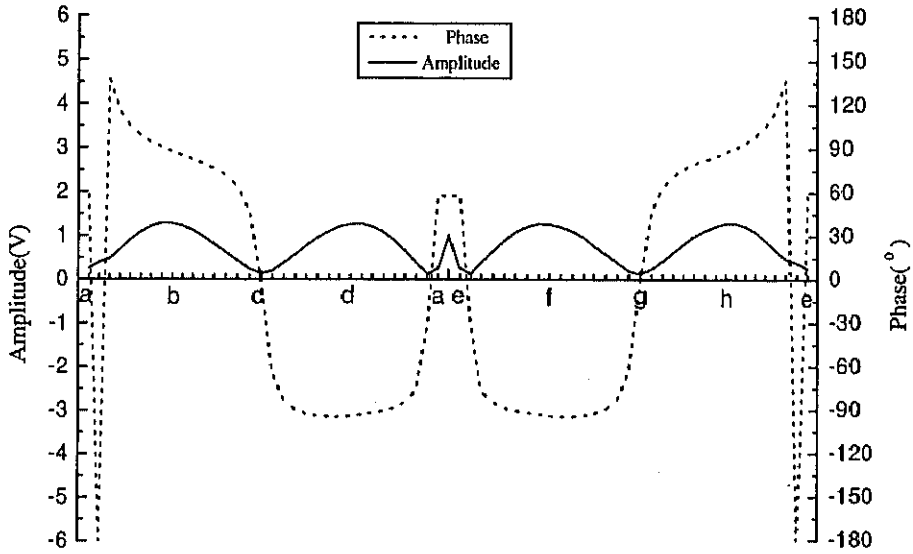

Fig. 3.20: Magnetic current distribution along the slot without short-circuiting points, where Xc=Yc=160mm, Zc=14mm, Xs=Ys=66mm, Dr=10mm, W=3mm, f_0=1.6GHz.

3.2.3 Antenna Characteristics

For the case with two short-circuiting points, the input impedance against frequency is given in Figs. 3.22 and 3.23. In Fig. 3.22, the different cavity depth Zc's 10mm, 14mm, and 18mm are chosen, respectively. In Fig. 3.23, the cavity width Xc's are 150mm, 160mm, and 170mm, respectively. It should be noted that the input impedance is not so sensitive to the cavity dimensions and the variation of input impedance is smoother than that of the single rectangular

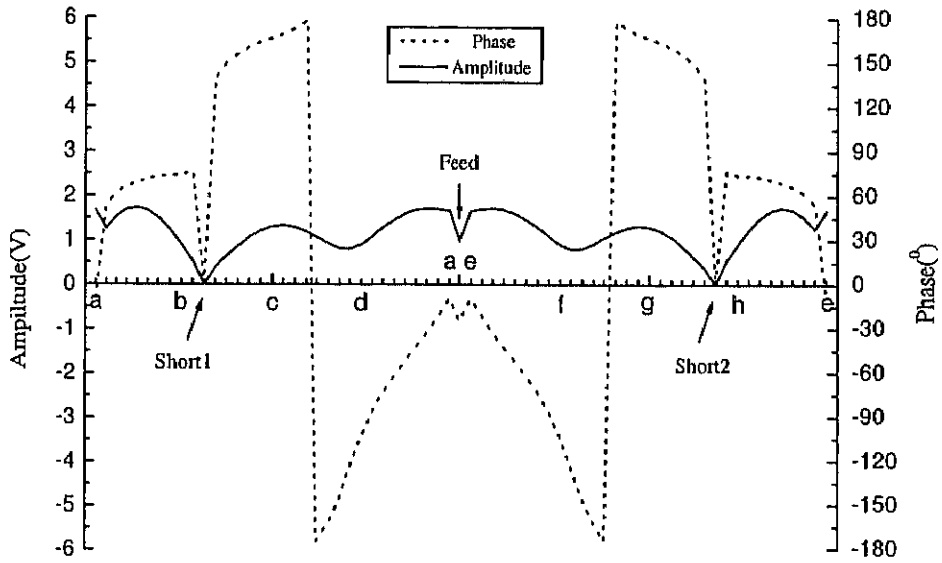

Fig. 3.21: Magnetic current distribution along the slot with short-circuiting points, where Xc=Yc=160mm, Zc=14mm, Xs=Ys=66mm, Dr=10mm, W=3mm, Ls=82mm, f_0=1.6GHz.

slot antenna.

As circularly polarized antennas, the axial ratio is one of very important characteristics. Figs. 3.24 and 3.25 show the axial ratio in the Z direction against frequency for different Zc and Xc, respectively. For comparison, the AR for the antenna without a cavity is also plotted in Fig. 3.24. Note that the axial ratio bandwidth ($\leq$3dB) of the cavity-backed antenna decreases to about 3% from 7% of that without the cavity. When Xc=0.853λ_0, Zc=0.075λ_0, Dr=0.053λ_0, Ls=0.44λ_0 and the total length of the slot is 2.816λ_0, the minimum axial ratio of 0.12dB is obtained at f_0=1.6GHz. From Figs. 3.24 and 3.25, it is also obvious that the effect of the cavity depth Zc on the axial ratio is more significant than that of the cavity width Xc. We also find that in Figs. 3.24 and 3.25 the center frequency is almost independent of Xc, but it is strongly dependent on Zc, which is similar to Figs. 3.9 and 3.10.

Figs. 3.26 and 3.27 give the radiation pattern and the axial ratio with respect to θ in the $\phi = 0°$, 45°, 90° and 135° planes at 1.6GHz, respectively.

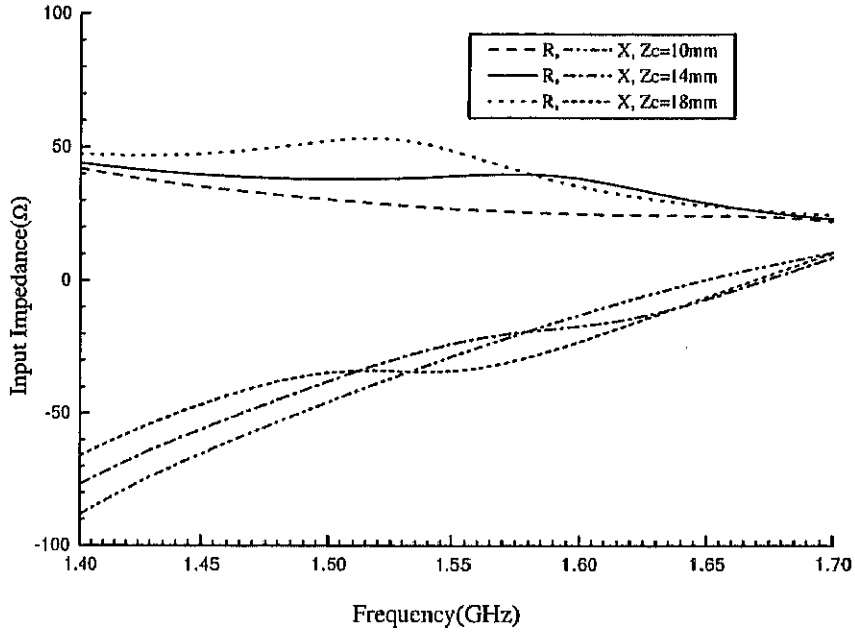

Fig. 3.22: Input impedance for different Zc, where Xc=Yc=160mm, Xs=Ys=66mm, Dr=10mm, W=3mm, Ls=82mm.

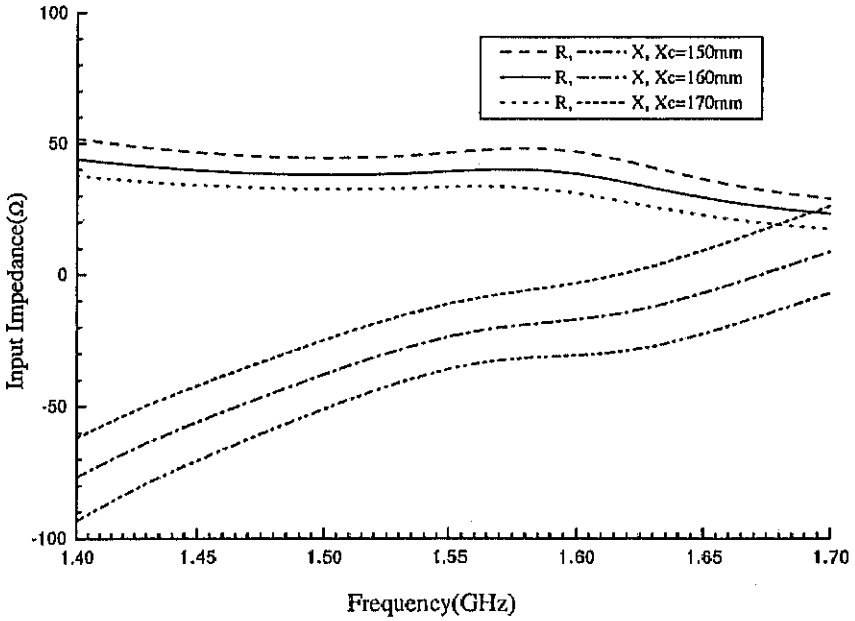

Fig. 3.23: Input impedance for different Xc, where Zc=14mm, Xs=Ys=66mm, Dr=10mm, W=3mm, Ls=82mm.

Because of the symmetric magnetic current distribution, the radiation patterns are symmetric with respect to the Z axis in each of the ϕ planes. The E_ϕ components are similar in all of the ϕ planes. The E_θ components in the $\phi = 0°$, 45° and 90° planes are similar and are greater than -6dB when $0° \leq \theta \leq 90°$. The E_θ component in the $\phi = 135°$ plane becomes -18dB when $\theta \geq 70°$. In Fig. 3.27, the axial ratios in different ϕ planes are shown. It is not difficult to see that the axial ratios with respect to θ are also symmetric to the Z axis and similar in the different ϕ planes. The axial ratio is less than 3dB for $-40° \leq \theta \leq 40°$.

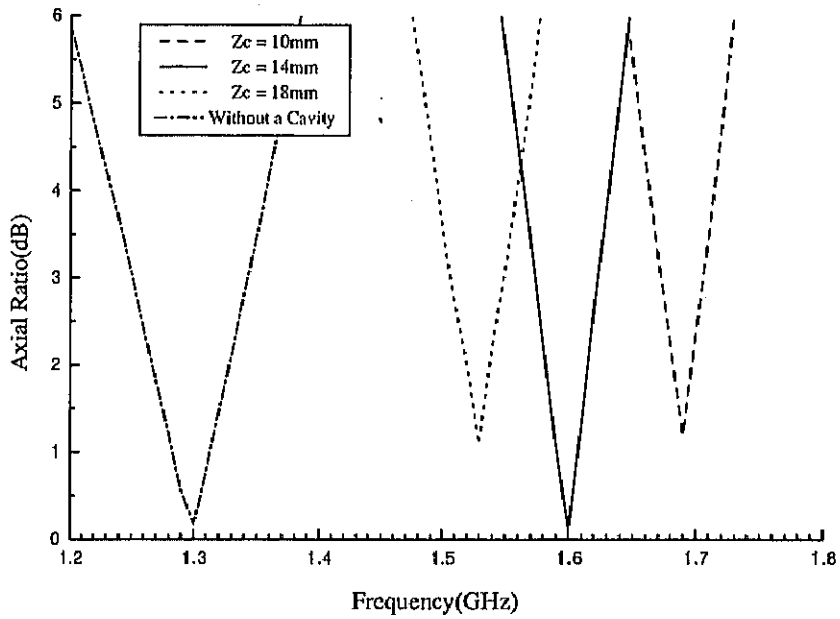

Fig. 3.24: Axial ratio for different Zc, where Xc=Yc=160mm, Xs=Ys=66mm, Dr=10mm, W=3mm, Ls=82mm.

For the rectangular-cavity-backed two-element square loop slot antenna, the optimized antenna dimensions for the circular polarization at f_0=1.6GHz (λ_0 = 187.5mm) are summarized in Table 3.3. From this table we can see that circular polarization occurs when the short-circuiting point is set $0.44\lambda_0$ from the feed point. The dimensions of the cavity also contribute to the occurrence of the circular polarization as can be seen in the next subsection.

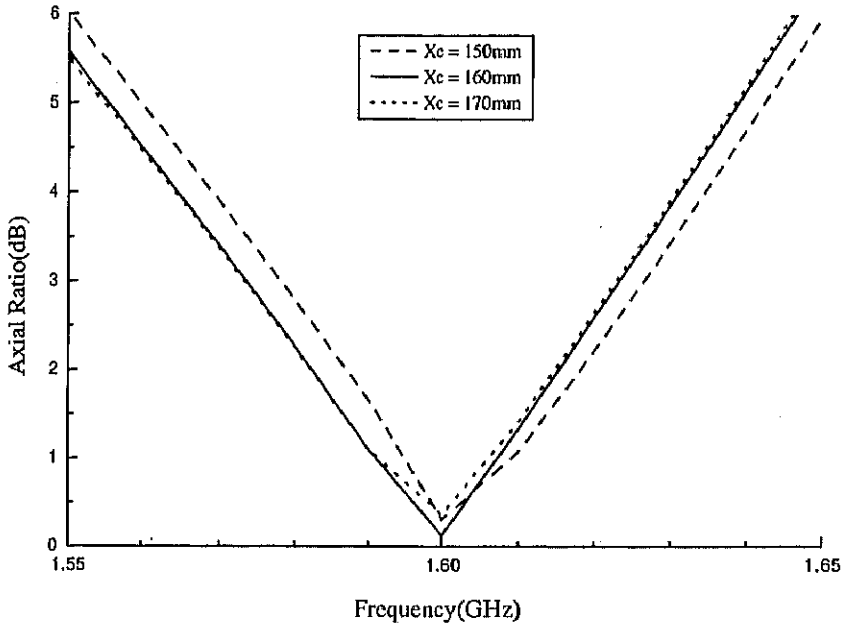

Fig. 3.25: Axial ratio for different Xc, where Zc=14mm, Xs=Ys=66mm, Dr=10mm, W=3mm, Ls=82mm.

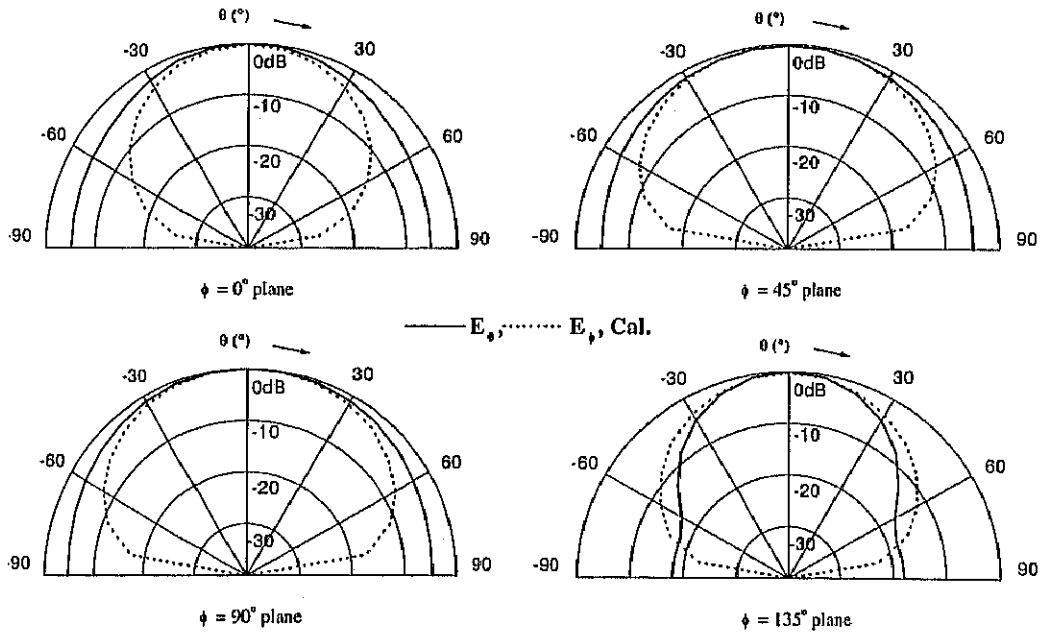

Fig. 3.26: Radiation patterns with short-circuiting points, where Xc=Yc=160mm, Zc=14mm, Xs=Ys=66mm, Dr=10mm, W=3mm, Ls=82mm, f_0=1.6GHz.

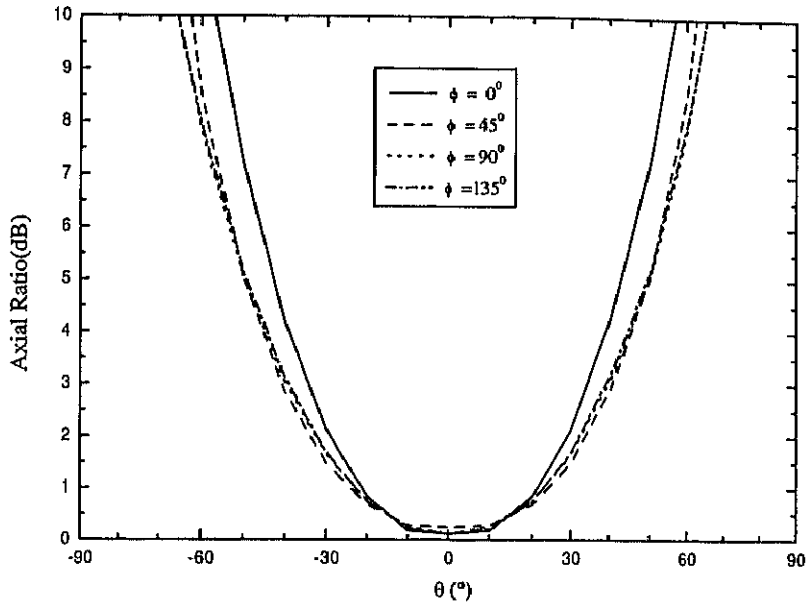

Fig. 3.27: Axial ratio with respect to θ in a constant ϕ plane, where Xc=Yc=160mm, Zc=14mm, Xs=Ys=66mm, Dr=10mm, W=3mm, Ls=82mm, f_0=1.6GHz.

Xc	Zc	4Xs	Dr	Ls
$0.853\lambda_0$	$0.075\lambda_0$	$1.41\lambda_0$	$0.053\lambda_0$	$0.44\lambda_0$

Table 3.3: Optimized antenna dimensions for circular polarization.

3.2.4 Experimental Results

To verify the analysis, the experiment on the input impedance, axial ratio and radiation pattern is performed. According to the discussion in the last subsection, the antenna dimensions are chosen as shown in Table 3.4. With these dimensions, the antenna is expected to radiate circularly polarized waves in the Z direction as calculated in the last subsection.

Xc	Yc	Zc	Xs	Ys	Dr	W	Ls
160mm	160mm	14mm	66mm	66mm	10mm	3mm	82mm

Table 3.4: Experimental dimensions of the rectangular-cavity-backed two-element square loop slot antenna.

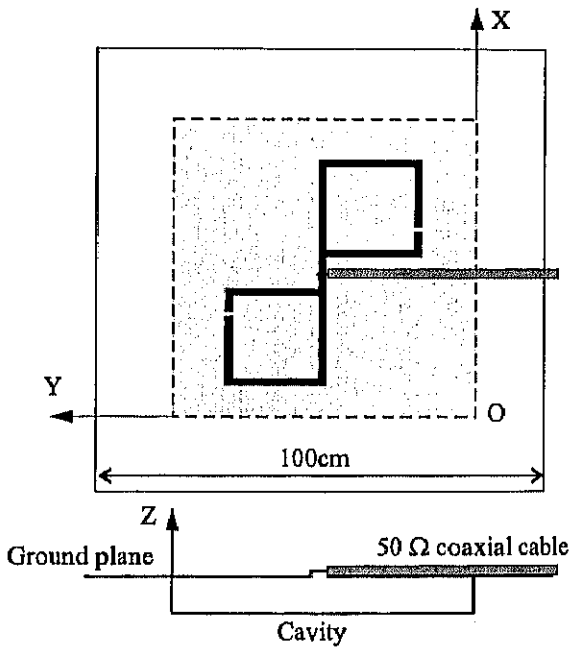

Fig. 3.28: Antenna structure in the experiment.

The antenna structure is shown in Fig. 3.28, where the antenna parameters and the way of feeding the slot by a 50 Ω semi-rigid coaxial cable are shown. In the experiment, a square copper plate of side 100cm and thickness 0.3mm is used as a ground plane. The two-element square loop slot is formed

on the ground plane. The cavity is also made by the cooper plate of thickness 0.3mm. The slot is shorted with two cooper sheets of width 1mm. The slot is fed by a semi-rigid coaxial cable along the ground plane to minimize the effect of the feed line. The frequency used is a 1.60GHz band.

The measured and calculated input impedance and axial ratio are plotted in Figs. 3.14 and 3.15, respectively. From Figs. 3.14 and 3.15, we find that the measured and calculated input impedance and axial ratio are in good agreement.

Fig. 3.31 shows the measured and calculated radiation patterns with respect to θ in the $\phi = 0°$ and 90° planes, respectively. The operating frequency is chosen as 1.60GHz. The calculated E_θ and E_ϕ in the $\phi = 0°$ and 90° planes are in good agreement with the measured results, except around $\theta = -90°$ and 90°. One of the reasons that the calculated results do not coincide with the measured ones around $\theta = -90°$ and 90° is the use of the finite-sized ground plane in the experiment.

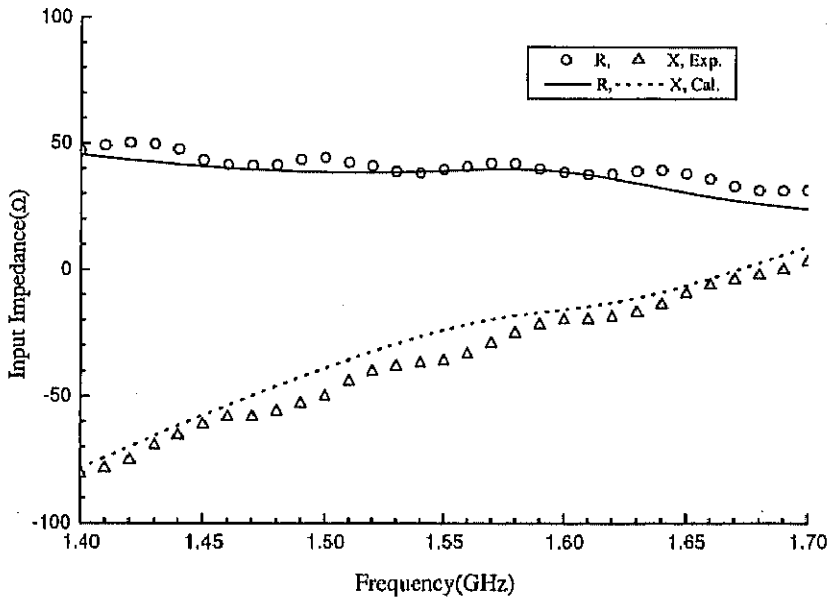

Fig. 3.29: The measured and calculated input impedance against frequency with short-circuiting points, where Xc=Yc=160mm, Zc=14mm, Xs=Ys=66mm, Dr=10mm, W=3mm, Ls=82mm.

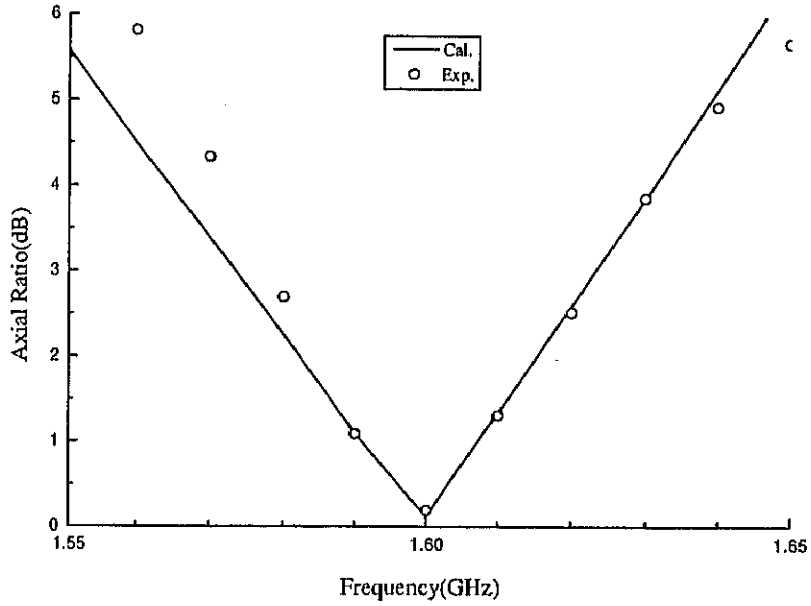

Fig. 3.30: The measured and calculated axial ratio against frequency with short-circuiting points, where Xc=Yc=160mm, Zc=14mm, Xs=Ys=66mm, Dr=10mm, W=3mm, Ls=82mm.

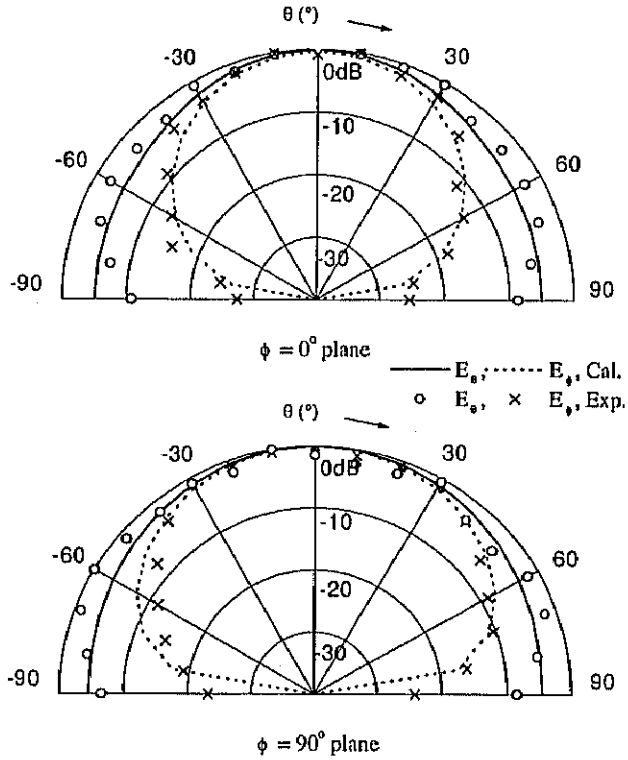

Fig. 3.31: The measured and calculated radiation patterns with short-circuiting points, where Xc=Yc=160mm, Zc=14mm, Xs=Ys=66mm, Dr=10mm, W=3mm, Ls=82mm, f_0=1.60GHz.

3.3 Rectangular-Cavity-Backed Two-Arm Square Spiral Slot Antenna

A cavity-backed spiral slot antenna is widely used as a circularly polarized low-profile antenna. The unidirectional and intrinsic traveling wave characteristics are attractive features, particularly when combined with its mechanical simplicity and compact size. In this section, a cavity-backed two-arm square spiral slot antenna is introduced to radiate circularly polarized waves, and in addition, symmetric radiation patterns are obtained due to its symmetric structure.

3.3.1 Antenna Structure

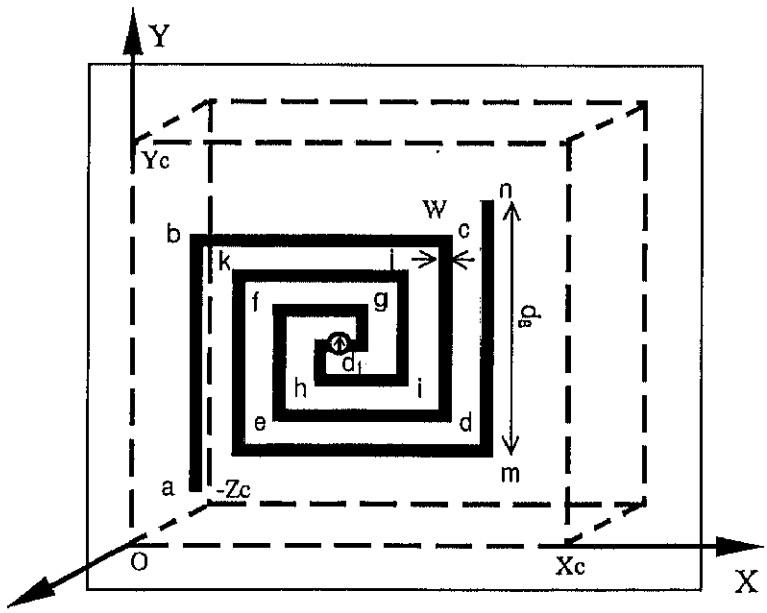

Fig. 3.32: Rectangular-cavity-backed two-arm square spiral slot antenna.

The two-arm square spiral slot is shown in Fig. 3.32. The two-arm square spiral slot is placed at the center of the cavity on the ground plane. The geometry of the slot is generated by $d_n = 2(n-1)d_1, (n = 2,3,\ldots,8)$, where

$d_1 = 0.04\lambda_0$ and n denotes the number of the turns of the single arm square spiral slot. In the calculation, the center frequency is chosen as 1.5GHz. A constant current i_0 is fed at the center of the two-arm square spiral slot (Xc/2, Yc/2, 0).

3.3.2 Circular Polarization Characteristics

The calculated magnetic current amplitude and its phase at 1.5GHz are shown in Fig. 3.33. The phase decreases linearly from the feed point to the two arm ends (except the region around the arm ends, owing to the reflection). The phase change is more linear than that of the rectangular-cavity-backed two-element square loop slot antenna, and the variation of the magnitude is also smaller than that of the rectangular-cavity-backed two-element square loop slot antenna. This is because the spiral antenna is a kind of typical traveling wave antenna. The axial ratio bandwidth ($\leq$3dB) of 4% with the minimum value of 0.2dB is obtained as shown in Figs. 3.34 and 3.35. From the two figures we can see that the axial ratio is sensitive to both Zc and Xc.

The radiation pattern and axial ratio with respect to θ are shown in Figs. 3.36 and 3.37, respectively. The E_ϕ component is almost the same as that of the two-element square loop slot antenna in Fig. 3.26. The E_θ components in all of the ϕ planes are symmetric with respect to the Z axis and greater than -10dB. In Fig. 3.37, as expected, the axial ratios with respect to θ are also symmetric to the Z axis and are similar in the different ϕ planes. The axial ratio is less than 3dB for $-50° \leq \theta \leq 50°$, which is wider than that of the rectangular-cavity-backed two-element square loop slot antenna.

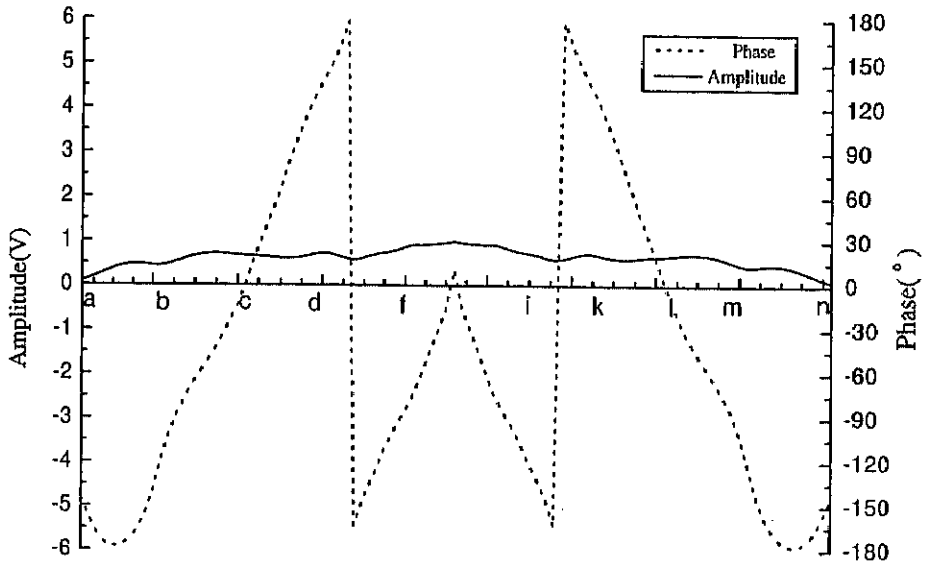

Fig. 3.33: Magnetic current distribution along the slot, where Xc=Yc=201mm, Zc=22mm, n=8, d_1=8mm, W=3mm, f_0=1.5GHz.

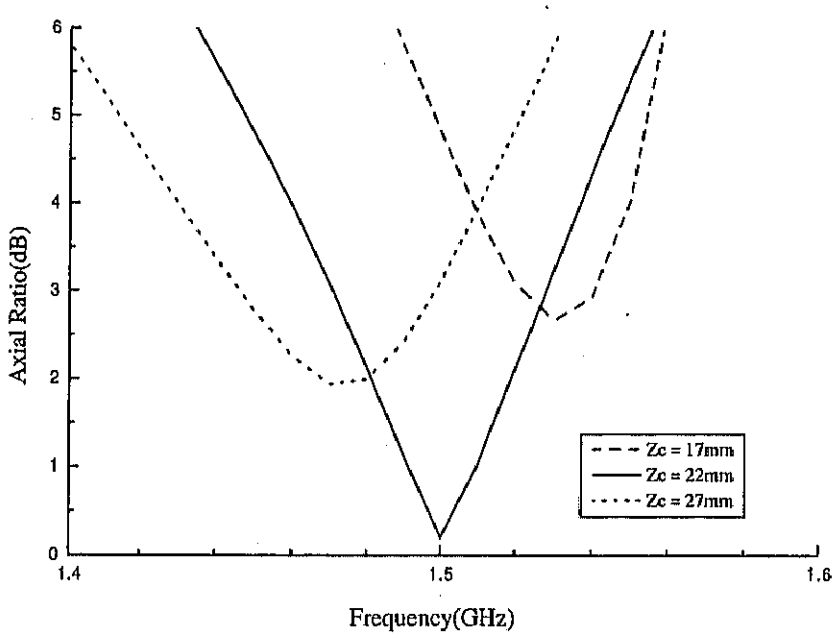

Fig. 3.34: Axial ratio for different Zc, where Xc=Yc=201mm, n=8, d_1=8mm, W=3mm.

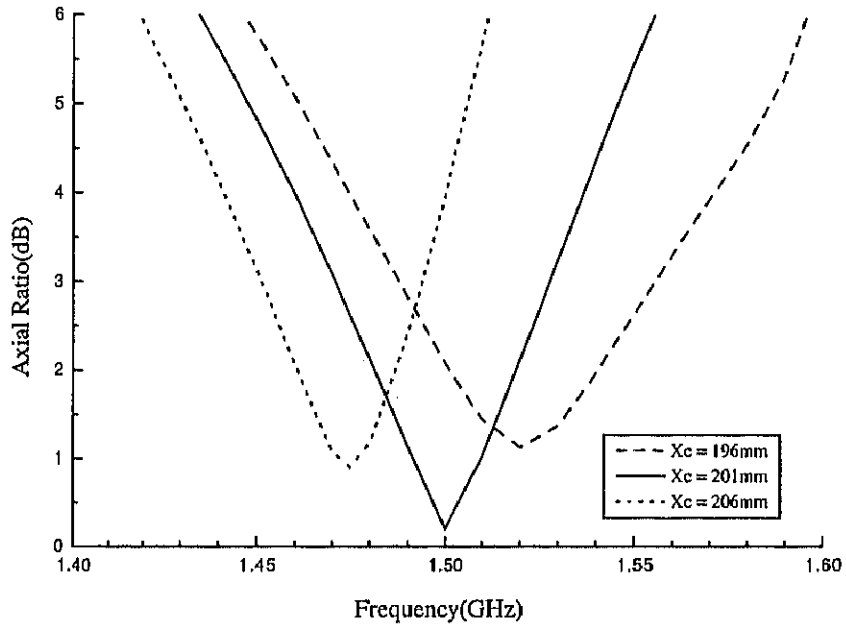

Fig. 3.35: Axial ratio for different Xc, where Zc=22mm, n=8, d_1=8mm, W=3mm.

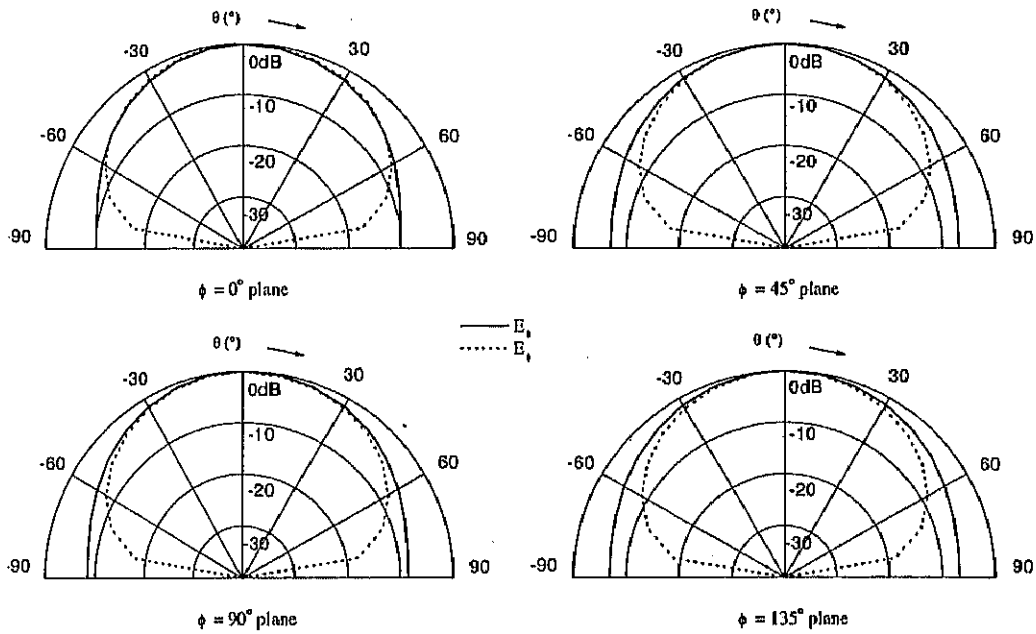

Fig. 3.36: Radiation patterns, where Xc=Yc=201mm, Zc=22mm, n=8, d_1=8mm, W=3mm, f_0=1.5GHz.

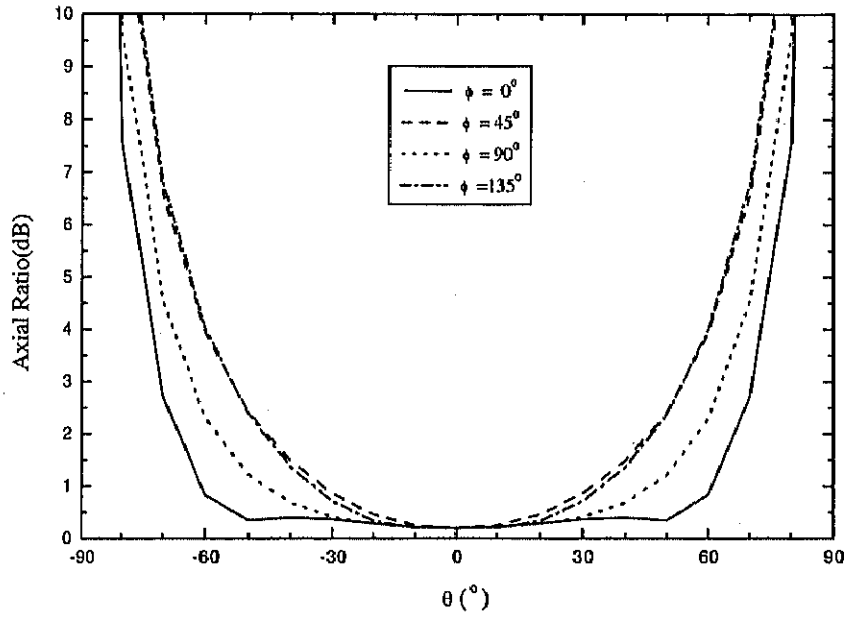

Fig. 3.37: Axial ratio with respect to θ in a constant ϕ plane, where Xc=Yc=201mm, Zc=22mm, n=8, d_1=8mm, W=3mm, f_0=1.5GHz.

3.4 Conclusions

Three types of the rectangular-cavity-backed slot antennas (a single square loop slot antenna, a two-element square loop slot antenna and a two-arm square spiral slot antenna) have been investigated. The discussion concentrates on the realization of circular polarization and the way of enhancing the radiation characteristics.

By applying the formulation derived in Chapter 2, the magnetic current distribution is obtained. The input impedance, radiation pattern and axial ratio are then calculated. The characteristics of the rectangular-cavity-backed single square loop slot antenna and the rectangular-cavity-backed two-element square loop slot antenna are examined numerically and experimentally. Further the rectangular-cavity-backed two-arm square spiral slot antenna is examined numerically. In this procedure, the computer program based on the formulation of Chapter 2 has been examined, which can be easily applied to other rectangular-cavity-backed slot antennas.

Based on the numerical and experimental study, three important observations can be made. First is that by short-circuiting the slot on appropriate positions, an expected travelling wave magnetic current appears partly on the slot, and good circular polarization and symmetric radiation patterns are achieved. It should be pointed out that the axial ratio and magnetic current distribution are very sensitive to the positions of the short-circuiting points. Second is that the effect of the backing cavity dimensions on the antenna characteristics is significant. Especially the axial ratio and the center frequency are very sensitive to the size of the backing cavity. However, the effect of the cavity size on the radiation pattern and even the input impedance is not so serious. The last one is that compared to the rectangular-cavity-backed single or two-element loop slot antenna, a rectangular-cavity-backed spiral slot antenna has a wider axial ratio bandwidth ($\leq$3dB) of 4% with the minimum value of 0.2dB and a more symmetric radiation pattern.